PAPER • OPEN ACCESS

Tunable second harmonic generation by an all-dielectric diffractive metasurface embedded in liquid crystals

To cite this article: Davide Rocco *et al* 2022 *New J. Phys.* **24** 045002

View the article online for updates and enhancements.

New Journal of Physics

The open access journal at the forefront of physics

Deutsche Physikalische Gesellschaft **DPG**

IOP Institute of Physics

Published in partnership with: Deutsche Physikalische Gesellschaft and the Institute of Physics

CrossMark

OPEN ACCESS

PAPER

Tunable second harmonic generation by an all-dielectric diffractive metasurface embedded in liquid crystals

Davide Rocco[1,2], Attilio Zilli[3], Antonio Ferraro[4], Adrien Borne[5], Vincent Vinel[5], Giuseppe Leo[5], Aristide Lemaître[6], Carlo Zucchetti[3], Michele Celebrano[3,*], Roberto Caputo[4,7], Costantino De Angelis[1,2] and Marco Finazzi[3]

1   Department of Information Engineering, University of Brescia, via Branze 38, Brescia 25123, Italy
2   National Institute of Optics (INO), via Branze 45, 25123 Brescia, Italy
3   Department of Physics, Politecnico di Milano, Piazza Leonardo Da Vinci 32, Milano 20133, Italy
4   Department of Physics & CNR-NANOTEC, University of Calabria, via P. Bucci, Cubo 31 C, Rende 87036, Italy
5   Université de Paris, CNRS, Laboratoire Matériaux et Phénomènes Quantiques, 75013 Paris, France
6   Université Paris-Saclay, CNRS, Centre de Nanosciences et de Nanotechnologies, 91120, Palaiseau, France
7   Institute of Fundamental and Frontier Sciences, University of Electronic Science and Technology of China, Chengdu 610054, People's Republic of China
*   Author to whom any correspondence should be addressed.
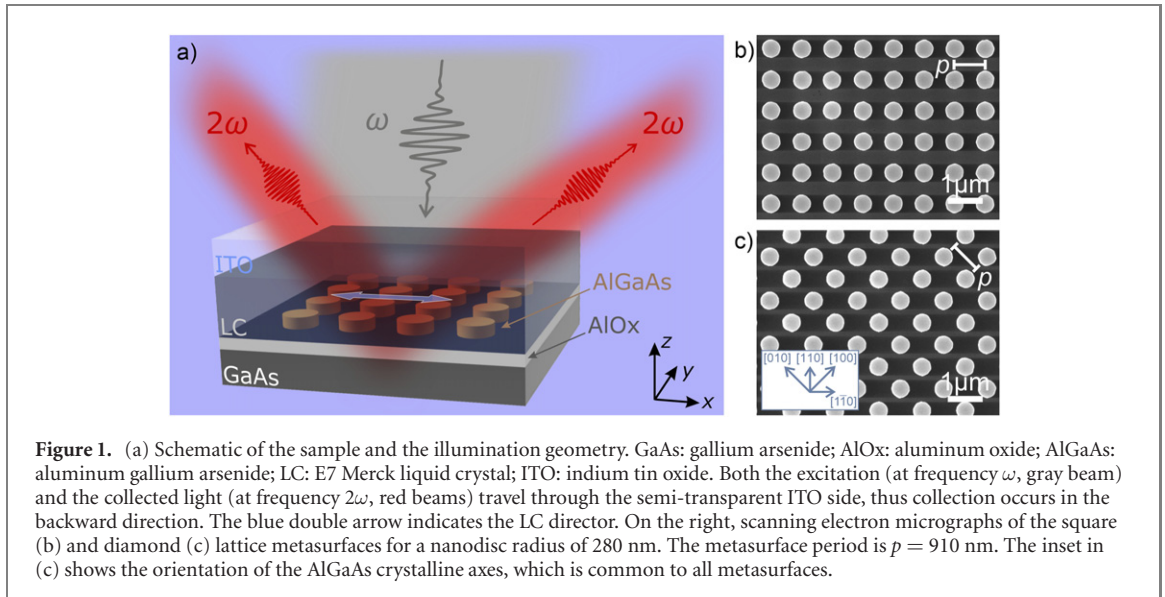
E-mail: michele.celebrano@polimi.it

Abstract

We experimentally demonstrate the possibility to modulate the second harmonic (SH) power emitted by nonlinear AlGaAs metasurfaces embedded in a liquid crystal (LC) matrix. This result is obtained by changing the relative in-plane orientation between the LC director and the linear polarization of the light at the excitation wavelength. According to numerical simulations, second-harmonic is efficiently radiated by the metasurfaces thanks to the sizeable second-order susceptibility of the material and the resonant excitation of either electric or magnetic dipole field distributions inside each meta-atom at the illuminating fundamental wavelength. This resonant behavior strongly depends on the geometric parameters, the crystallographic orientation, and the anisotropy of the metasurface, which can be optimized to modulate the emitted SH power by about one order of magnitude. The devised hybrid platforms are therefore appealing in view of enabling the electrical control of flat nonlinear optical devices.

1. Introduction

All-dielectric metasurfaces are attracting increasing interest from the scientific community for optical wavefront manipulation [1–3]. The possibility of controlling the phase of the light scattered by each unit of the metasurface and the lossless nature of the optical resonances in high refractive index dielectric nanostructures are key assets [4, 5]. A wide range of applications including lenses, beam deflectors and holograms have been shown [6–9]. The considerable potential of these devices has stimulated the demonstration of tunable metasurfaces [10] and several mechanisms have been proposed to reach this goal. A straightforward realization of tunable metasurfaces relies on mechanical deformations to reconfigure the entire structure [11, 12]. For instance, the authors of reference [12] have proposed an array of dielectric resonators embedded in an elastomeric matrix, where remarkable optical resonance shifts have been experimentally demonstrated to stem from the application of uniaxial strain. Another appealing strategy to attain reconfigurability is to fabricate metasurfaces out of phase change materials (e.g. chalcogenides, correlated oxides), whose optical properties strongly depend on the application of an external electric field stimulus [13, 14]. Faster control mechanisms have also been reported, such as the ultrafast photo-injection of a dense electron–hole plasma into a dielectric Mie-resonant nanoparticle [15, 16], leading to femtosecond transient dielectric permittivity. The possibility to thermally tune the metasurface behavior has also been proposed, owing to optical heating of single all-dielectric nanoantennas [17–19]. In this context,

Figure 1. (a) Schematic of the sample and the illumination geometry. GaAs: gallium arsenide; AlOx: aluminum oxide; AlGaAs: aluminum gallium arsenide; LC: E7 Merck liquid crystal; ITO: indium tin oxide. Both the excitation (at frequency ω, gray beam) and the collected light (at frequency 2ω, red beams) travel through the semi-transparent ITO side, thus collection occurs in the backward direction. The blue double arrow indicates the LC director. On the right, scanning electron micrographs of the square (b) and diamond (c) lattice metasurfaces for a nanodisc radius of 280 nm. The metasurface period is $p = 910$ nm. The inset in (c) shows the orientation of the AlGaAs crystalline axes, which is common to all metasurfaces.
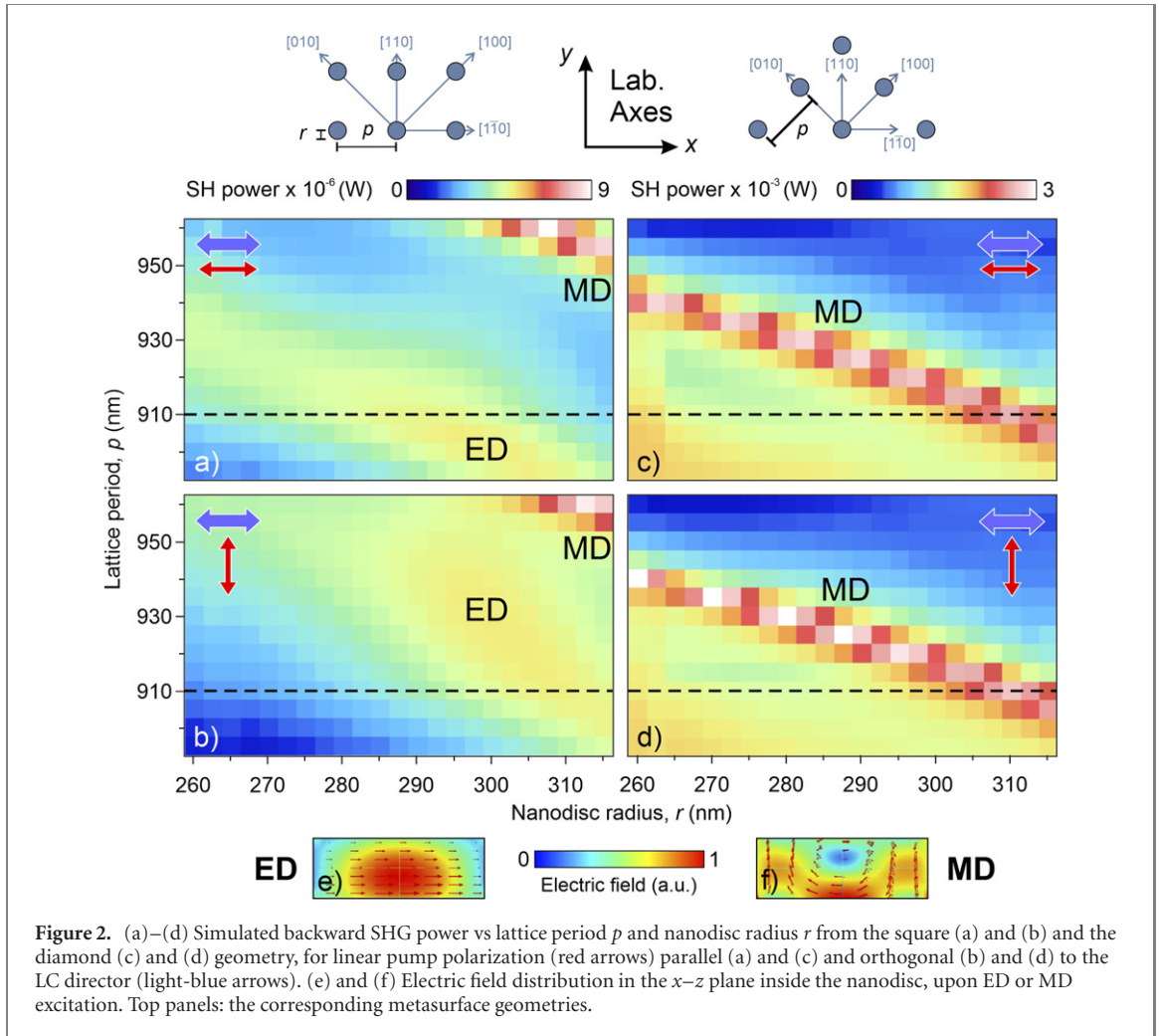
LCs represent valid candidates for the implementation of tunable metasurfaces thanks to their high birefringence ($n_e - n_o \sim 0.2$), which can be controlled by temperature or by an externally applied electric field [20–23]. Moreover, LC-based metasurfaces might profit from well-established fabrication techniques developed for the display industry [24–26]. The re-shaping of the light scattered from a dielectric metasurface as a function of the orientation of the liquid crystal (LC) director has been thoroughly investigated in the linear regime and already exploited to realize ultracompact gas sensors [27]. Conversely, the control of the nonlinear harmonic signals generated by metasurfaces embedded in LC matrices is still at an early stage. In this scenario, we recently discussed the possibility to obtain a SHG modulator by using a commercial LC as the immersion medium of a high-refractive index metasurface made of AlGaAs nanodiscs over an AlOx substrate [28]. Our numerical simulations show that the SHG can be switched on or off by changing the LC director from the *planar* to the *homeotropic* (namely, out of the metasurface plane) alignment.

Here, we discuss and experimentally demonstrate the modulation of the SHG from an optimized dielectric metasurface embedded in a LC matrix, as a function of the relative orientation between the incident pump beam ($\lambda = 1551$ nm) polarization and the LC director kept *in the plane* of the metasurface (see figure 1(a)). As a result, for a well-defined orientation of the array with respect to the crystallographic axes and optimized geometrical parameters of the metasurface, we obtained a second harmonic (SH) emitted power that is about one order of magnitude higher when the pump polarization is switched from collinear to orthogonal to the LC director. These results pave the way to ultrathin nonlinear modulators where the LC anisotropy is electrically, thermally, or optically controlled.

2. Numerical simulations

To assess the combined effect of the relative orientation of the AlGaAs crystalline axes and the metasurface lattice with respect to the LC director, we have investigated two geometries with AlGaAs nanodiscs, having thickness of 200 nm, as meta-atoms arranged in a square lattice with axes parallel to either (i) the [110] and [1$\bar{1}$0] crystallographic directions (square geometry, figure 1(b)) or (ii) the [100] and [010] (diamond geometry, figure 1(c)), with the director always parallel to [1$\bar{1}$0]. To find indications on the geometry enabling a large SH modulation, we have simulated the nonlinear optical response of such metasurfaces as a function of the radius r of each nanodisc, lattice period p, and orientation of the pump linear polarization. We have performed finite-element method simulations using the commercial software COMSOL Multiphysics. The unitary cell consists of a dielectric AlGaAs disc lying on an AlOx substrate, with refractive indices $n \simeq 3.4$ and $n = 1.6$, respectively, in the wavelength range of interest. To model the E7 LC matrix that surrounds each nanopillar, we assumed a homogeneous anisotropic dielectric medium with extraordinary and ordinary refractive indices $n_e = 1.6$ and $n_o = 1.5$, respectively, at both pump and SH wavelength. In fact, although in this wavelength for the E7 LCs $n_e = 1.69$ and $n_o = 1.5$ [29], we found that a reduced anisotropy such as the one above, allows to attain a better match between simulations and experimental data (see section 4). Such a reduced LC anisotropy, indeed, better depicts a realistic situation

Figure 2. (a)–(d) Simulated backward SHG power vs lattice period *p* and nanodisc radius *r* from the square (a) and (b) and the diamond (c) and (d) geometry, for linear pump polarization (red arrows) parallel (a) and (c) and orthogonal (b) and (d) to the LC director (light-blue arrows). (e) and (f) Electric field distribution in the *x*–*z* plane inside the nanodisc, upon ED or MD excitation. Top panels: the corresponding metasurface geometries.

in which the effects of disorder at room temperature and a specific anchoring of the LC molecules to the nanodiscs cannot be neglected.

The pump beam was described as a plane wave incident normal to the substrate with a wavelength $\lambda = 1551$ nm. To model the SH emission, we simulated in the frequency domain the scattered field distribution at the pump frequency ω to determine the SH sources in terms of current densities. Given the zincblende crystalline structure ($F\bar{4}3m$ crystallographic space group) of AlGaAs, the *i*th Cartesian component of the external current density J_i is calculated as:

$$J_i(2\omega) = j\omega_{\mathrm{SH}}\varepsilon_0\chi_{ijk}^{(2)}E_j(\omega)E_k(\omega)$$

with $i \neq j \neq k$, ε_0 the vacuum permittivity, $E_i(\omega)$ the *i*th Cartesian component of the electric field at ω, and $\chi_{ijk}^{(2)}$ the second-order susceptibility, which in the case of AlGaAs was set to 200 pm V^{-1} [30]. In our simulations the dielectric nanodiscs were the sole sources of SH since both the LC and the AlOx substrate have negligible $\chi^{(2)}$ [31].

Figure 2 displays the calculated overall SH emitted power in the backward direction for a metasurface period, *p*, varying from 895 nm to 960 nm. In this range, SHG is dominated by the metasurface resonances associated with either an electric dipole (ED) or a magnetic dipole (MD) field distribution at ω inside each nanodisc (see figures 2(e) and (f)) [28]. It is worth noting that, in the investigated region of the parameter space, the ED is the main responsible for SH enhancement in the square geometry (see figures 2(a) and (b)), while the MD constitutes the major contribution to SHG in the diamond geometry (see figures 2(c) and (d)). One can readily notice that these resonances significantly depend on the lattice period *p*, a behavior that indicates some degree of near-field coupling between meta-atoms. In addition, while the MD resonance is much sharper than the ED due to its lower radiative losses, it shows a weak dependence on the relative orientation between the LC director and the pump polarization. Conversely, although weaker and broader, the ED resonance is strongly affected by how the director is oriented with respect to the light polarization and is, therefore, very promising in view of SH modulation. To verify this concept, we compare

the two geometries for $p = 910$ nm (see black dashed lines in figure 2), where the ED contribution to the SH emission is expected to be stronger.
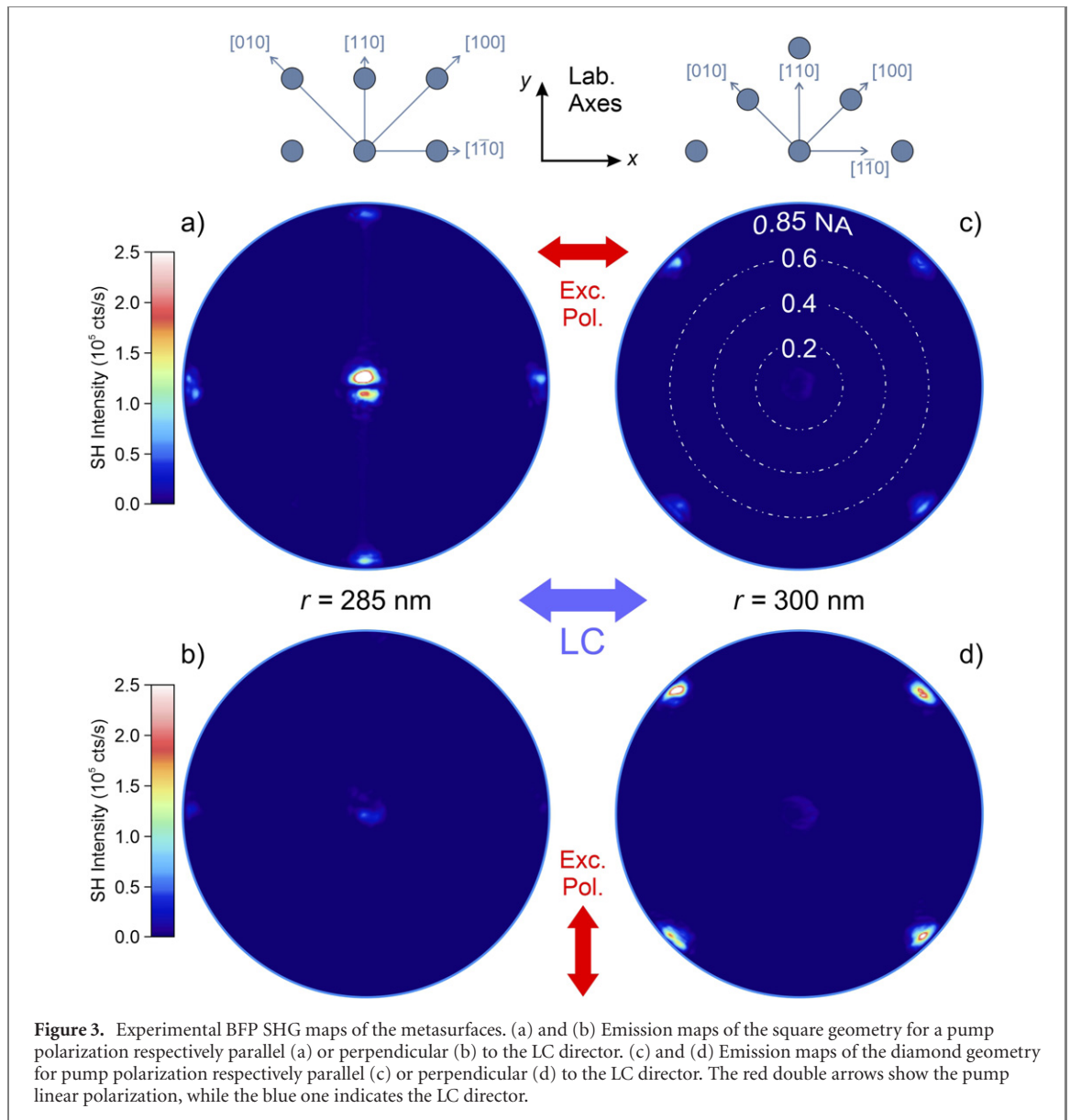
3. Sample fabrication

Metasurfaces were fabricated, similarly to reference [32], starting from a 1 μm-thick $Al_{0.98}Ga_{0.02}As$ film and a 200 nm-thick layer of $Al_{0.18}Ga_{0.82}As$ successively grown on a GaAs substrate by molecular beam epitaxy. The nanostructures are lithographically patterned out of the $Al_{0.18}Ga_{0.82}As$ layer. A final step of selective oxidation of the Al-rich film creates a low-index AlOx layer, which is essential to attain effective field confinement in the meta-atoms. To investigate the effect of the meta-atom geometry on the SHG yield and rule out possible fabrication inaccuracies that might result in systematic variations of the sizes with respect to nominal values, a set of metasurfaces with both square and diamond lattice configurations was fabricated with nanodisc radius varying from 260 to 315 nm and $p = 910$ nm. Representative scanning electron micrographs of the two configurations are shown in figures 1(b) and (c), respectively. The crystallographic axes of AlGaAs in the images are oriented as indicated in the inset of panel c.

The metasurfaces were subsequently embedded in a 12 μm-thick E7 LC matrix using the following procedure. To exploit the full birefringence of the LC, the first step is to adopt an alignment layer that enables a preferential direction of the LC molecules in the rest condition. A solution of Poly(vinyl alcohol) 0.5% wt in distilled water is thus spin-coated at 3000 rpm for 30 s on both the metasurface substrate and the ITO superstrate. We would like to point out that, although in this paper we perform static measurements without an external applied voltage, we adopted a cell design with an ITO superstrate in view of future voltage dependent studies. Then the sample is baked at 120 °C for 1 h, resulting in an alignment layer of few tens of nanometers thickness. Successively, a rubbing machine is used to rub the polymer layer along a specific direction, using a rotating drum covered by a cloth with short fibers. The device is eventually assembled by sandwiching the treated metasurface with an ITO cover slip as superstrate, put at controlled distance by means of a 12 μm thick mylar spacer. The obtained cell is sealed with UV glue, taking care to leave two opposite entrances, for the following LC filling step (during the cell assembly, attention is devoted to lay it down on the metasurface with parallel alignment direction). To prevent the formation of air bubbles, the filling process is performed in a vacuum chamber at a temperature of 80 °C, well above the clearing point of the LC. Finally, the device is slowly cooled down and the open entrances are sealed with UV glue. This last choice has two advantages: (i) avoid the LCs to pour out from the cell and (ii) keep their alignment fixed.

4. Results and discussion

To investigate the nonlinear emission of the metasurfaces, we employed a home-made confocal microscope coupled with an ultrafast pump laser with emission centered at $\lambda = 1551$ nm and delivering 160 fs pulses at 80 MHz repetition rate (OneFive Origami, NKT Photonics). The experimental setup was already described elsewhere (see reference [33] for details). Briefly, to excite the whole metasurface, the fundamental pump beam is focused to the back-focal-plane (BFP) of a $60\times$ objective (Nikon, CFI Plan Fluor 60XC, numerical aperture, NA = 0.85) mounted on-axis to obtain a collimated beam that impinges at normal incidence on the sample. A zero-order half-wave retarder working at the pump wavelength is inserted in the excitation path to rotate the polarization of the pump beam. The emitted SH is collected through the same objective used for the excitation, and chromatically filtered using a narrow band-pass filter centered at 775 nm (bandwidth 25 nm). A Bertrand lens inserted in the detection path images the SH diffraction orders in the BFP of the objective onto a cooled CCD camera (iKon M-934, Andor Technology). The average excitation power employed is 10 mW, which corresponds to an average power density on the sample of about 2 kW cm^{-2} based on a beam diameter of about 25 μm. The employed excitation wavelength, which lies in the transparency window of the investigated materials, along with the low power density level, prevents any temperature-induced nematic-isotropic transition in the LC.

The periodic arrangement of the nanodiscs in the metasurface combined with the interference of the coherent SHG by each individual meta-atom results in a directional beaming of SH in the first diffraction orders of the metasurface, which acts as a diffraction grating for the SHG. According to Bragg's diffraction law with a period $p = 910$ nm, the first SH diffraction orders are expected at an angle $\alpha = \sin^{-1}\left(\frac{775 \text{ nm}}{910 \text{ nm}}\right) \cong 58°$, which falls just within the numerical aperture of our collection objective (NA $\cong 0.85$). The nonlinear BFP maps featuring the highest SHG yield are shown in figure 3 as a function of the relative orientation of the linear pump polarization with the LC director, for both the square and diamond metasurface geometries. The first diffraction orders fall at the edge of the objective NA and are therefore partially cut off.

Figure 3. Experimental BFP SHG maps of the metasurfaces. (a) and (b) Emission maps of the square geometry for a pump polarization respectively parallel (a) or perpendicular (b) to the LC director. (c) and (d) Emission maps of the diamond geometry for pump polarization respectively parallel (c) or perpendicular (d) to the LC director. The red double arrows show the pump linear polarization, while the blue one indicates the LC director.

In figure 3, one can observe SH emission around the normal direction (especially visible in panel a). As previously observed, selection rules forbid normal emission for a single AlGaAs nanodisc [34], but the metasurface periodicity allows to attain sizeable emission in the paraxial direction also for normal incidence excitation [35]. Moreover, also spurious effects might appear in the paraxial direction due to possible fabrication tolerances [36]. However, in the following we will solely focus on the effects on first diffraction orders.

It can be readily noticed that, in the square geometry, the SH power is significantly higher in panel a, namely when the pump polarization is parallel to the LC director. In this case the SHG power is enhanced by a factor 7 for all the first diffraction orders with respect to the value obtained for an orthogonal alignment between the pump polarization and the director (panel (b)). In the diamond geometry (panels (c) and (d)) the SH power modulation is more than a factor 2 less pronounced, with higher yield corresponding to a pump polarization orthogonal to the LC director. We stress that in both geometries the relative orientation between the crystal axis of AlGaAs and the pump polarization is kept fixed to rule out possible effects associated with the $\chi^{(2)}$ tensor of the material.

We have then recorded a series of BFP maps as a function of the nanodisc radius and pump polarization to compare experimental evidence to the simulations in figure 2 and confirm the physical mechanism behind the observed modulation. Figure 4(a) shows the radius-dependent SH emitted power integrated over all the first diffraction order by the metasurfaces featuring a square geometry. Each data point represents a different metasurface, where r is varied from 260 to 315 nm, while p is set at 910 nm. From these plots we conclude that, by changing the polarization of the pump beam from parallel (blue curve) to
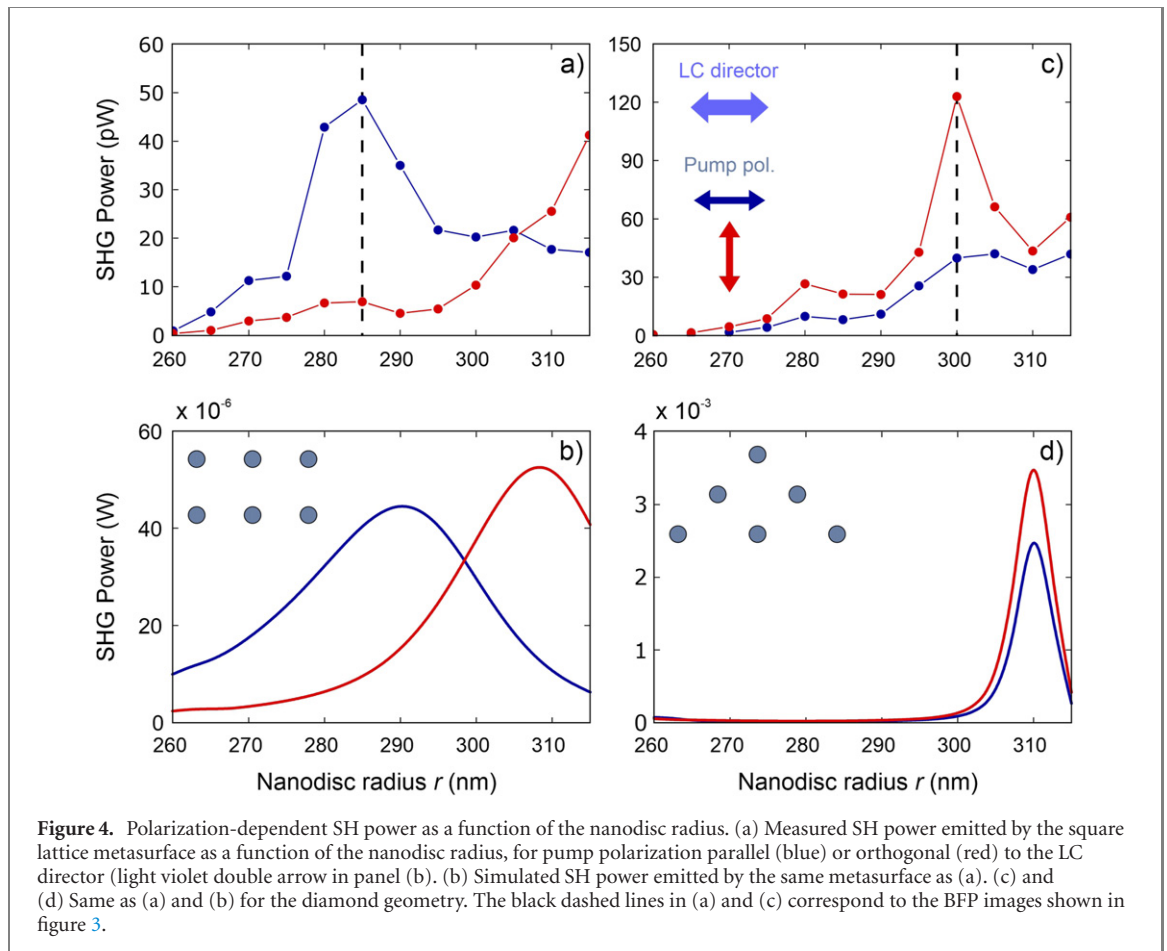
Figure 4. Polarization-dependent SH power as a function of the nanodisc radius. (a) Measured SH power emitted by the square lattice metasurface as a function of the nanodisc radius, for pump polarization parallel (blue) or orthogonal (red) to the LC director (light violet double arrow in panel (b). (b) Simulated SH power emitted by the same metasurface as (a). (c) and (d) Same as (a) and (b) for the diamond geometry. The black dashed lines in (a) and (c) correspond to the BFP images shown in figure 3.

perpendicular (red curve) with respect to the LC director, the condition for optimal SH emission significantly changes, shifting to longer radii. As previously mentioned, we ascribe this behavior to the non-negligible near-field coupling between the meta-atoms (see figure 2), which causes a sizeable shift of the ED as a function of the LC/surrounding refractive index at the excitation wavelength. Thereby, for a fixed meta-atom radius of 285 nm, we can attain a SH power modulation up to almost one order of magnitude. Both these features are well reproduced by the simulations, reported for comparison in figure 4(b). In particular, the blue and the red plots correspond to the white dashed line drawn in figures 2(a) and (b), respectively, which indicate the SH simulated power for $p = 910$ nm.

In figure 4(c) are shown measurements performed on the diamond geometry, where—at variance with the square case—changing the orientation of the pump polarization does not affect the MD resonance (i.e. the radius of the resonating nanodisc) but rather the total SH power. Even in this case the numerical simulations are in good qualitative agreement with the experiment. Yet, the experimental data in the co-polarized configuration do not show a peak as pronounced as in the simulations. This could be attributed to small deviations of the nanodisc radii from the nominal values as well as to a possible nanodisc ellipticity introduced by the fabrication process. We would also like to point out that the LC orientation, which has a key role in the SH emission, is extremely sensitive to the local anchoring to the metasurface and, therefore, might be affected by the sample morphology itself. This phenomenon, which is critical to control and investigate in detail, might introduce uncertainties in the experiments, such as the discrepancy reported above. Nevertheless, the combination of experiments and simulations indicates that, while the diamond geometry is more efficient in directing SH power to the first diffraction order, it is less sensitive to the LC anisotropy. Finally, we would like to point out that the SH in the experiments is several orders of magnitude lower than the numerical prediction—most markedly so for the diamond lattice. This quantitative mismatch can be ascribed to the significant power drop caused by the unavoidable spatial selection imparted by the finite NA of our objective, but also to the fact that numerical simulations were conducted in the CW regime using a single wavelength coherent pump excitation, while ultrafast broadband pulse excitation was employed in the experiment.

5. Conclusions

We have experimentally demonstrated that the SHG power from a nonlinear metasurface embedded in a LC matrix can be modulated by about one order of magnitude by changing the relative orientation between the LC director and the pump polarization. In our experimental realization, the fundamental-wavelength beam impinges normal to the metasurface, and the modulation is performed by keeping both the LC director and the illumination field in the plane of the metasurface. This represents a convenient geometry, which could enable the electrical control of the SH emission with bias electrodes fabricated directly on top of the metasurface. Our numerical simulations indicate that the SHG is ruled by electric and MD field distributions inside each meta-atom at the pump wavelength, which depend on the geometrical parameters and the crystallographic orientation of the metasurface as well as on the anisotropy of the environment.

Numerical simulations also suggest that one can leverage many degrees of freedom to tune the nonlinear properties of the metasurface. Indeed, the size and shape of the meta-atoms, their near-field coupling, the orientation of the meta-atom lattice with respect to the AlGaAs crystallographic axes, the exciting polarization, and the orientation of the LC director are all parameters that strongly affect the SH emission by the metasurface, offering large flexibility and the possibility to find optimal solutions for a wide range of applications of nonlinear optics with flat devices.

Data availability statement

The data that support the findings of this study are available upon reasonable request from the authors.

ORCID iDs

Davide Rocco ⓘ https://orcid.org/0000-0002-5678-0531
Attilio Zilli ⓘ https://orcid.org/0000-0003-1845-6850
Antonio Ferraro ⓘ https://orcid.org/0000-0003-0189-6729
Adrien Borne ⓘ https://orcid.org/0000-0001-9320-7091
Giuseppe Leo ⓘ https://orcid.org/0000-0001-6525-6734
Aristide Lemaître ⓘ https://orcid.org/0000-0003-1892-9726
Carlo Zucchetti ⓘ https://orcid.org/0000-0002-0428-5184
Michele Celebrano ⓘ https://orcid.org/0000-0003-3336-3580
Roberto Caputo ⓘ https://orcid.org/0000-0002-0065-8422
Costantino De Angelis ⓘ https://orcid.org/0000-0001-8029-179X
Marco Finazzi ⓘ https://orcid.org/0000-0002-9197-3654

References

[1] Overvig A C, Shrestha S, Malek S C, Lu M, Stein A, Zheng C and Yu N 2019 Dielectric metasurfaces for complete and independent control of the optical amplitude and phase *Light: Sci. Appl.* **8** 1–12
[2] Liu W, Li Z, Cheng H and Chen S 2020 Dielectric resonance-based optical metasurfaces: from fundamentals to applications *Iscience* **23** 101868
[3] Qiu C, Zhang T, Hu G and Kivshar Y 2021 Quo vadis, metasurfaces? *Nano Lett.* **21** 5461–74
[4] Genevet P, Capasso F, Aieta F, Khorasaninejad M and Devlin R 2017 Recent advances in planar optics: from plasmonic to dielectric metasurfaces *Optica* **4** 139–52
[5] Albella P, Poyli M A, Schmidt M K, Maier S A, Moreno F, Sáenz J J and Aizpurua J 2013 Low-Loss electric and magnetic field-enhanced spectroscopy with subwavelength silicon dimers *J. Phys. Chem.* C **117** 13573–84
[6] Shresta S, Overvig A C, Lu M, Stein A and Yu N 2018 Broadband achromatic dielectric metalenses *Light: Sci. Appl.* **7** 1–11
[7] Zhao R, Xiao X, Geng G, Li X, Li J, Li X, Wang Y and Huang L 2021 Polarization and holography recording in real- and *k*-space based on dielectric metasurface *Adv. Funct. Mater.* **31** 2100406

[8] Guo Z, Zhu L, Shen F, Zhou H and Gao R 2017 Dielectric metasurface based high-efficiency polarization splitters *RSC Adv.* **7** 9872–9

[9] Zhang Q, Li M, Liao T and Cui X 2018 Design of beam deflector, splitters, wave plates and metalens using photonic elements with dielectric metasurface *Opt. Commun.* **411** 93–100

[10] He Q, Sun S and Zhou L 2019 Tunable/reconfigurable metasurfaces: physics and applications *Research* **2019** 1–16

[11] Cataldi U, Caputo R, Kurylyak Y, Klein G, Chekini M, Umeton C and Bürgi T 2014 Growing gold nanoparticles on a flexible substrate to enable simple mechanical control of their plasmonic coupling *J. Mater. Chem.* C **2** 7927–33

[12] Gutruf P, Zou C, Withayachumnankul W, Bhaskaran M, Sriram S and Fumeaux C 2016 Mechanically tunable dielectric resonator metasurfaces at visible frequencies *ACS Nano* **10** 133–41

[13] Zhang Y *et al* 2021 Electrically reconfigurable non-volatile metasurface using low-loss optical phase-change material *Nat. Nanotechnol.* **16** 661–6

[14] Wang Y, Landreman P, Schoen D, Okabe K, Marshall A, Celano U, Wong H-S P, Park J and Brongersma M L 2021 Electrical tuning of phase-change antennas and metasurfaces *Nat. Nanotechnol.* **16** 667–72

[15] Makarov S, Kudryashov S, Mukhin I, Mozharov A, Milichko V, Krasnok A and Belov P 2015 Tuning of magnetic optical response in a dielectric nanoparticle by ultrafast photoexcitation of dense electron–hole plasma *Nano Lett.* **15** 6187–92

[16] Pogna E A A *et al* 2021 Ultrafast, all optically reconfigurable, nonlinear nanoantenna *ACS Nano* **15** 11150–7

[17] Zograf G P, Petrov M I, Zuev D A, Dmitriev P A, Milichko V A, Makarov S V and Belov P A 2017 Resonant nonplasmonic nanoparticles for efficient temperature-feedback optical heating *Nano Lett.* **17** 2945–52

[18] Aouassa M *et al* 2017 Temperature-feedback direct laser reshaping of silicon nanostructures *Appl. Phys. Lett.* **111** 243103

[19] Celebrano M *et al* 2021 Optical tuning of dielectric nanoantennas for thermo-optically reconfigurable nonlinear metasurfaces *Opt. Lett.* **46** 2453–6

[20] Bohn J, Bucher T, Chong K E, Komar A, Choi D-Y, Neshev D N, Kivshar Y S, Pertsch T and Staude I 2018 Active tuning of spontaneous emission by mie-resonant dielectric metasurfaces *Nano Lett.* **18** 3461–5

[21] Komar A *et al* 2017 Electrically tunable all-dielectric optical metasurfaces based on liquid crystals *Appl. Phys. Lett.* **110** 071109

[22] Komar A, Paniagua-Domínguez R, Miroshnichenko A, Yu Y F, Kivshar Y S, Kuznetsov A I and Neshev D 2018 Dynamic beam switching by liquid crystal tunable dielectric metasurfaces *ACS Photonics* **5** 1742–8

[23] Zou C, Komar A, Fasold S, Bohn J, Muravsky A A, Murauski A A, Pertsch T, Neshev D N and Staude I 2019 Electrically tunable transparent displays for visible light based on dielectric metasurfaces *ACS Photonics* **6** 1533–40

[24] Schadt M 1997 Liquid crystal materials and liquid crystal displays *Annu. Rev. Mater. Sci.* **27** 305–79

[25] Birendra B 1984 Liquid crystal displays *Mol. Cryst. Liq. Cryst.* **109** 3–93

[26] Chen H-W, Lee J-H, Lin B-Y, Chen S and Wu S-T 2018 Liquid crystal display and organic light-emitting diode display: present status and future perspectives *Light: Sci. Appl.* **7** 17168

[27] Kim I *et al* 2021 Holographic metasurface gas sensors for instantaneous visual alarms *Sci. Adv.* **7** eabe9943

[28] Rocco D, Carletti L, Caputo R, Finazzi M, Celebrano M and De Angelis C 2020 Switching the second harmonic generation by a dielectric metasurface via tunable liquid crystal *Opt. Express* **28** 12037–46

[29] Li J, Wu S-T, Brugioni S, Meucci R and Faetti S 2005 Infrared refractive indices of liquid crystals *J. Appl. Phys.* **97** 073501

[30] Gili V F *et al* 2016 Monolithic AlGaAs second-harmonic nanoantennas *Opt. Express* **24** 15965–71

[31] Kim H-W, Mun J-H, Yoon C-S and Kim J-D 2001 Second harmonic generation and photorefractive effect in dye-doped liquid crystals *Jpn. J. Appl. Phys.* **40** L952–4

[32] Gigli C, Marino G, Suffit S, Patriarche G, Beaudoin G, Pantzas K, Sagnes I, Favero I and Leo G 2019 Polarization- and diffraction-controlled second-harmonic generation from semiconductor metasurfaces *J. Opt. Soc. Am.* B **36** E55–64

[33] Tognazzi A *et al* 2021 Third-harmonic light polarization control in magnetically resonant silicon metasurfaces *Opt. Express* **29** 11605–12

[34] Camacho-Morales R *et al* 2016 Nonlinear generation of vector beams from AlGaAs nanoantennas *Nano Lett.* **16** 7191–7

[35] Marino G, Gigli C, Rocco D, Lemaître A, Favero I, De Angelis C and Leo G 2019 Zero-order second harmonic generation from AlGaAs-on-insulator metasurfaces *ACS Photonics* **6** 1226–31

[36] Gili V F *et al* 2018 Role of the substrate in monolithic AlGaAs nonlinear nanoanennas *Nanophotonics* **7** 517–21